Int. J. Electrochem. Sci., 13 **(2018)** 4561 – 4574, doi: 10.20964/2018.05.68

International Journal of ELECTROCHEMICAL SCIENCE
www.electrochemsci.org

Facile Synthesis of Mn_2O_3 for Highly Active Catalytic Oxidation and Reduction of Organic Substances and Electrochemical Determination of L-Methionine

Ragu Sasikumar[1], Tse-Wei Chen[1], Shen-Ming Chen[1,], Syang-Peng Rwei[2], Ming-Chin Yu[3, 4*]*

[1] Department of Chemical Engineering and Biotechnology, National Taipei University of Technology, No. 1, Section 3, Chung-Hsiao East Road, Taipei 106, Taiwan, ROC.
[2] Institute of Organic and Polymeric Materials, National Taipei University of Technology, No. 1, Section 3, Chung-Hsiao East Road, Taipei 106, Taiwan, ROC.
[3] Department of Surgery, Chang Gung Memorial Hospital, Taoyuan 333, Taiwan, ROC.
[4] Department of Surgery, Xiamen Chang Gung Hospital, Xiamen, Fujian, China
[*]E-mail: smchen78@ms15.hinet.net, mingchin2000@gmail.com

Received: 16 January 2018 / *Accepted:* 10 March 2018 / *Published:* 10 April 2018

This paper reports the electrochemical determination of L-Methionine (L-Met) in phosphate buffer solution (pH = 7.0) utilizing the Mn_2O_3 on screen-printed carbon electrode (Mn_2O_3/SPCE) and Mn_2O_3 catalyst display excellent activity for catalytic reduction of p-Nitrophenol. Initially, as-prepared Mn_2O_3 were characterized by various analytical methods. From the electrochemical studies bare SPCE showed an ill-defined oxidation peak around 1.214 (±0.02) V for L-Met whereas Mn_2O_3/SPCE showed a well-defined oxidation peak at 1.173 (±0.02) V. Under optimum conditions, the Mn_2O_3/SPCE showed a linear range of L-Met concentrations of 1.0 x 10^{-6} to 6.1 x 10^{-4} M. The limit of detection is about 1.0 x 10^{-9} M (S/N = 3). The presently modified working electrode has also been effectively applied for the determination of L-Met in real sea food samples. The Mn_2O_3 signifies user-friendly, strong and high sensitive with real applications for electrochemical determination of amino acids as well as catalytic reduction of p-Nitrophenol.

Keywords: Manganese oxide, amino acid, L-Methionine, p-Nitrophenol, Wild Salman.

1. INTRODUCTION

Due to the structural, compositional flexibility, and excellent physicochemical properties of Manganese oxide, is considered to be a technologically significant material in catalysis, magnetism, molecular adsorption, high power batteries, electronics, and chemical sensing contrivances etc., [1-16]. It possesses different oxidation states of 2+, 3+, 4+, and 6+. Amongst them, MnO_2 is one of the

predominant manganese oxide phases, and its applications as electrode materials in primary Li/MnO_2 batteries, catalysts in ion sieves as well as in electrochemical capacitors [17–23]. The preparation of MnO_2 is difficult techniques due to its problematical designates of process control. Many synthesis procedures available for MnO_2 such as reduction process [24], sol-gel [25], thermal oxidation [26], and chemical co-precipitation [27]. Manganese oxide employed an important role in electrochemical biosensors in recent years. Recent years, scientists were reported numerous electrochemical sensors based on MnO_2 [28-30].

Most of the animals, and plants have sulphur involved chemical compounds and them performance a vital role in the active system [31]. L-methionine (L-Met) have sulphur-attached protein genic amino acids. It originates and avoids the infections in hair, and skin. It is a considerable amino acid and consequential role for living methylation reactions. By incrementing lecithin engenderment, L-Met is utilized to reduce the cholesterol level and additionally paramount for human magnification [32]. Deficiencies of L-Met have been attributed to muscle paralysis, toxemia, despondency, and reduced magnification [33]. Above-mentioned astringent effects of L-Met, the dosage level must be quantified in pharmaceutical performs. Accordingly, the purpose of L-Met is very consequential in the medical perspective. The electrochemical method has remarkable receptiveness due to its great selectivity and sensitivity, quick response, low cost, and simple procedure. From the literature survey there is many oxidation studies reported for L-Met by betokens of different modified working electrodes such as an electro-polymerized film of non-peripheral amine superseded Cu(II) phthalocyanine [34], poly (3-amino-5-mercapto-1,2,4-triazole) [35], colloidal-gold cysteamine [36], and poly (methyl violet) [37]. The chemical structure of L-Methionine as exhibited in Scheme 1.

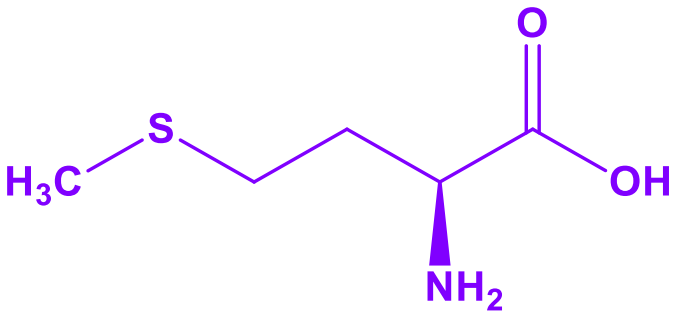

Scheme 1. Chemical structure of L-Met.

The main objective of this work is to develop a sensitive method for the detection of L-Met predicated on Mn_2O_3/SPCE for the first time. The prepared Mn_2O_3 was characterized by different physico-chemical techniques. It was tenacious the L-Met with the limit of detection (LOD) is about 1 nM. We additionally demonstrated the practical applicability of accurate sample analysis in wild Salman, and Shrimp (spiked) samples predicated on Mn_2O_3 modified SPCE and found acceptable instaurations.

2. EXPERIMENTAL SECTION

2.1. Materials

Manganese acetate tetrahydrate [$Mn(OAc)_2.4H_2O$] (>99%), N, N'-dimethylformamide (DMF) (99.8%), acetone (99.7%), and L-Methionine (L-Met) (≧98%) were obtained from Sigma-Aldrich. All the chemicals, reagents, and solvents used were of analytical grade. De-ionized water was used throughout the experiments.

2.2. Methods

2.2.1. Synthesis of Mn_2O_3

Initially, 0.091 g of [$Mn(OAc)_2.4H_2O$] was dissolved in 67.5 mL of DMF under constant stirring, and 7.5 mL of DI water was added to get a final concentration of 5 x 10^{-3} M. The yellowish-brown solution was stirred at 49 °C for 1 h and the resulting solution was left to stand for 3 months under at room temperature. After 3 months, the dark brown precipitate was obtained. The obtained precipitate was centrifuged, and washed several times with DI water and acetone to remove excess surfactant from the solution, and then dried in air at 120 °C for 30 minutes.

2.2.2. Fabrication of Mn_2O_3/SPCE

5 mg of Mn_2O_3 was well dispersed in 1 mL water under ultrasonic treatment for 1 h. On the surface of SPCE, the optimized concentration of about 8 µL of a dispersed solution was drop cast on the active surface of the SPCE followed by drying in an air oven at 30 °C for 1 h.

2.2.3. Characterization

The crystal structure, and surface morphology of the as-synthesized Mn_2O_3 were studied by powder X-ray diffraction (XPERT-PRO; PANalytical B.V., Netherlands). The morphology and elemental mapping of the as-synthesized composite were studied by scanning electron microscopy (SEM Hitachi S-3000 H) attached with energy-dispersive X-ray analyzer, respectively. Cyclic voltammetry (CV), and differential pulse voltammetry (DPV) were performed on electrochemical analyzer (CHI 400, and 900; CH Instruments). In this present work we have used three electrode system, SPCE as a modified working electrode, saturated Ag/AgCl as a reference electrode, and Pt wire as a counter electrode. For whole electrochemical experiments were carried out in N_2 saturated, 0.05 M phosphate buffer solution (PBS) as a supporting electrolyte was prepared from Na_2HPO_4, and NaH_2PO_4.

3. RESULTS AND DISCUSSION

3.1. Structural properties

Fig. 1 shows that the Mn_2O_3 diffraction peaks are detected at 2θ ca. 23.1° (211), 32.9° (222), 38.1° (400), 45.0° (332), 49.3° (431), 55.0° (440), and 65.7° (622) of Mn_2O_3 can be well correlated with pure Mn_2O_3 (JCPDS #24-0508) [38-40]. For Mn_2O_3, no other peaks were noticed from extra phases, proposing that the as-synthesized Mn_2O_3 are of high purity.

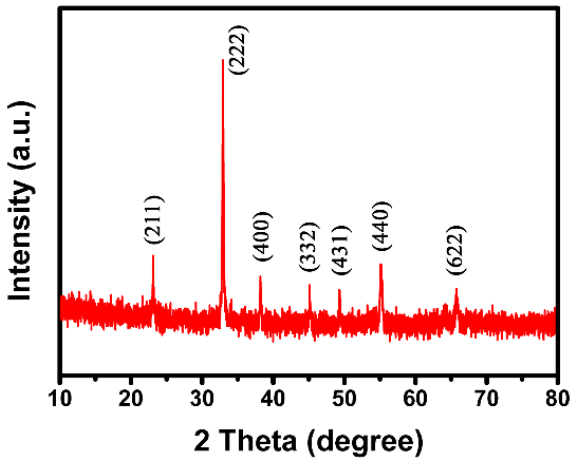

Figure 1. PXRD pattern for Mn_2O_3.

SEM with EDX analysis studied the structural, and elemental composition of the as-prepared Mn_2O_3. SEM images of prepared Mn_2O_3 is shown in Fig. 2 (A). It is seen that, Mn_2O_3 micro-clusters are not uniformly spread. The spectrum of EDX, elemental color mapping for synthesized Mn_2O_3 are shown in Fig. 2 (B-D). The spectrum shows the peaks equivalent to manganese and oxygen. The results confirm the purity of as-synthesized micro-clusters with no chemical impurities [37].

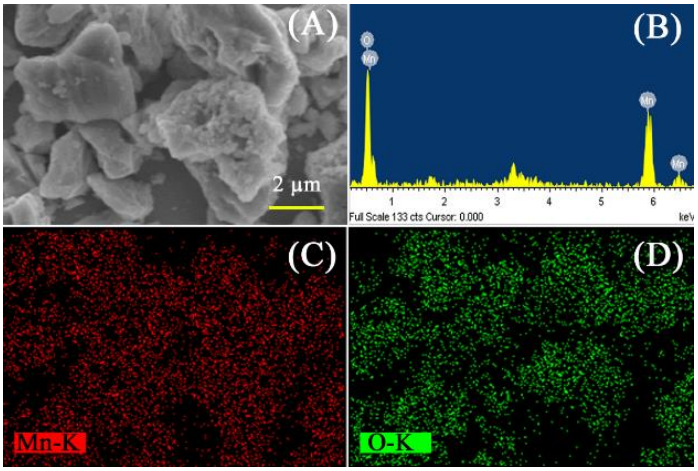

Figure 2. (A) SEM image, (B) EDS spectrum, and (C, D) elemental color mapping of the prepared Mn_2O_3.

The textural properties of the Mn_2O_3 sample were studied by N_2 adsorption/desorption isotherm, as shown in Fig. 3. The Mn_2O_3 sample showed isotherm curve close to the typical type III (IUPAC classification) isotherm. Therefore, a Brunauer-Emmett-Teller (BET) surface area of Mn_2O_3 sample was *ca.* 2.48 m^2 g^{-1}. The above result tells the probability of as-prepared Mn_2O_3 sample with satisfactory surface area.

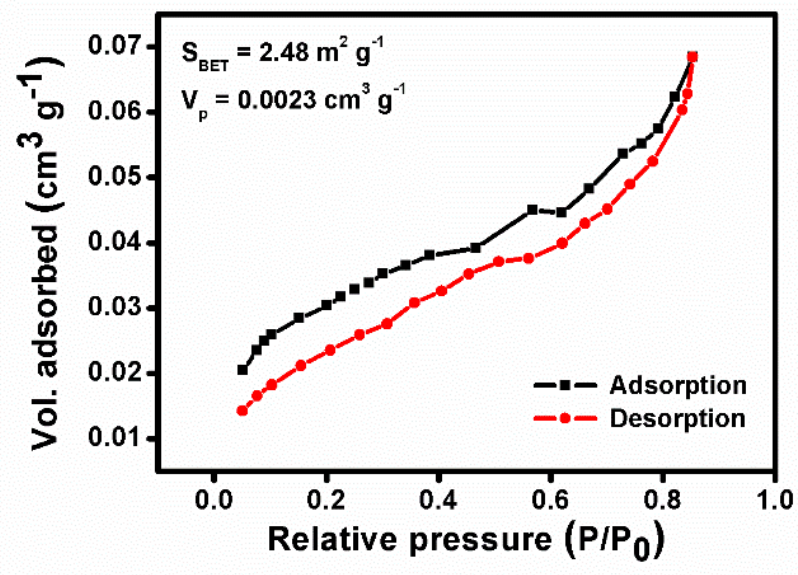

Figure 3. N_2 adsorption/desorption isotherm for Mn_2O_3.

3.2. Electro-catalytic oxidation of L-Met at Mn_2O_3/SPCE

Before studying the electro-catalytic oxidation property of the modified SPCE film towards L-Met, we have examined the electrochemical behavior of Mn_2O_3/SPCE in 0.05 M PBS. CV obtained for bare SPCE and Mn_2O_3 modified SPCE in 0.05 M PBS (pH 7) at a scanning rate of 50 mV s^{-1} is shown in Fig. 4. There is no visible peak appeared when introduced SPCE into the electrochemical setup. It shows that a small difference in the CV curve with a small peak potential (1.214 V) at E_{pa} (anodic peak potential), and also a small current by the addition of L-Met in bare SPCE. The well-marked anodic peak potential (E_{pa}) were detected at 1.173 V for the Mn_2O_3/SPCE. There is a no reduction peak appeared when the addition of L-Met. This result shows that the electrochemical behavior of L-Met is irreversible process. The oxidation mechanism of L-Met is shown in Scheme 2. However, Mn_2O_3/SPCE is showed maximum electro-oxidation performance compared to bare SPCE in terms of less over potential and high peak currents. Thus, Mn_2O_3/SPCE has a greater electro-oxidation ability to the oxidation of L-Met due to the good properties of conductivity and satisfactory surface area of the Mn_2O_3. The big anodic peaks happen at peak potentials of 1.173 V due to $2e^-$ oxidation of the L-Met. From the CV curves definitely that the Mn_2O_3/SPCE is a good electro-oxidation towards the L-Met.

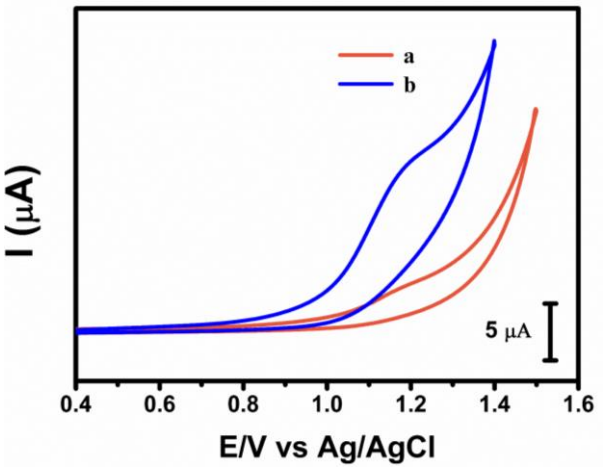

Figure 4. CVs obtainted of (a) bare SPCE, and (b) Mn_2O_3/SPCE in N_2 saturated 200 µM L-Met containing PBS at the scanning rate of 50 mV s^{-1}.

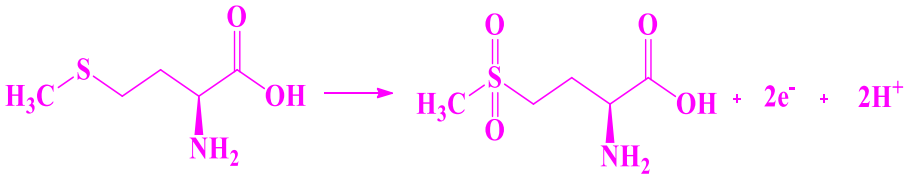

Scheme 2. Oxidation mechanism of L-Met.

3.3. Influence of L-Met addition

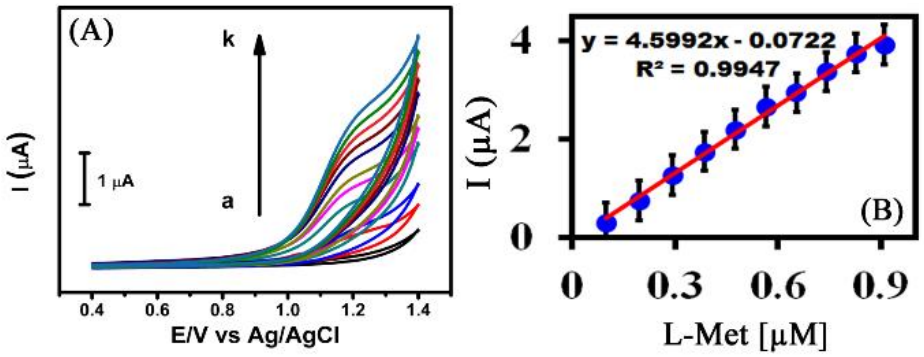

Figure 5. CVs obtained of (A) Mn_2O_3/SPCE different concentrations of L-Met (a = absence; b-k = 100-1000 µM L-Met, and (B) plot of oxidation peak current versus the concentration of L-Met in N_2 saturated PBS at the scanning rate of 50 mV s^{-1}.

Fig. 5A shows CV responses of Mn_2O_3/SPCE in PBS containing different concentrations of L-Met in N_2 saturated at a scanning rate of 50 mV s^{-1}. When the absence of L-Met, (a) the Mn_2O_3/SPCE does not show any visible peaks; whereas, a well-defined oxidation peak was observed in the presence of 100 µM L-Met. Moreover, the L-Met concentration from 100 to 1000 µM (b-k) increased means the oxidation peaks current of L-Met also increased. The results reveal that the excellent electro-oxidation

behavior of L-Met at Mn_2O_3/SPCE, and can be used for sensitive determination of L-Met. Fig. 5B demonstrates the plot between oxidation peak current, and L-Met concentrations, which may be communicated by a linear regression equation as E_{pa} (V) = 4.5992x – 0.0722, R^2 = 0.9947.

3.4. Influence of scanning rates

Fig. 6A shows that the effect of scanning rate of electro-catalytic oxidation responses of Mn_2O_3/SPCE in PBS (pH 7) for the determination of L-Met. The CV curves observed the oxidation peak currents are gradually increased when increasing the anodic peaks from 20 to 200 mV s^{-1}. When the oxidation peaks current (I_{pa}) increases the scanning rates also increases linearly which may be communicated by a linear regression equation as E_{pa} (V) = 0.032x – 0.0063, R^2 = 0.9977. Additionally, the linear plot among oxidation peak current versus the square root of the scanning rates has displayed a relationship which suggesting that the oxidation process of L-Met appeared at the Mn_2O_3/SPCE is a diffusion controlled electron transfer process Fig. 6B. From the results, we approve that the observed CV reports are due to the determination of L-Met diffused on the surface of the Mn_2O_3/SPCE.

$$LOD=3S_b/b \qquad \text{------- 1}$$

The LOD is calculated by using the above formula, slope of the straight line of the electrochemical analytical curve and SD of the mean value for ten voltammograms of the blank (S_b).

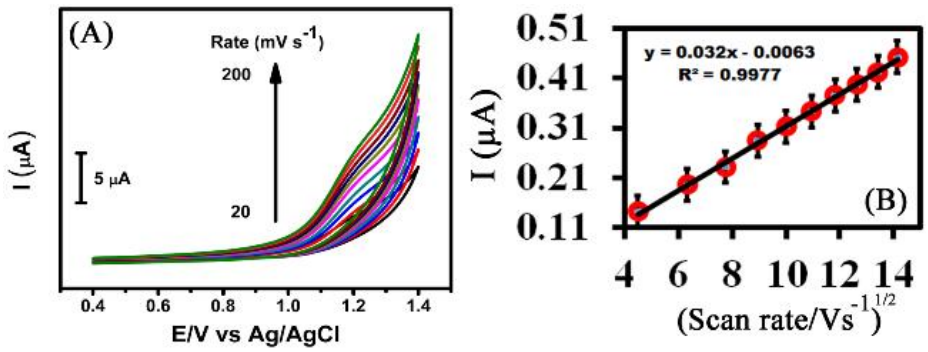

Figure 6. CVs obtained of (A) Mn_2O_3/SPCE different scanning rates of 200 µM L-Met from 20 to 200 mV s^{-1}, and (B) plot of oxidation peak current versus the square root of the scanning rates in N_2 saturated PBS at the scanning rate of 50 mV s^{-1}.

3.5. Calibration curve, and limit of detection

The electrochemical oxidation of L-Met was done at Mn_2O_3/SPCE by DPV. The DPV technique is a more sensitive method for the detection of L-Met than CV. The DPV responses of the Mn_2O_3/SPCE with the additions of various concentration of L-Met (1.0 x 10^{-6} M to 6.1 x 10^{-4} M) into the PBS (pH 7). The sensitivity was calculated by using the slope of the calibration plot as shown in the Fig. 7A. The lower concentrations as shown in Fig. 7B the calculated sensitivity was about 6.036 (±0.002) µA μM^{-1} cm^{-2}. The LOD is about 1.0 x 10^{-9} M observed from the slope of the calibration plot as shown in Fig. 7C. The linear relationship between L-Met concentration vs peak current (I_{pa}) was

obtained using 1.0 x 10^{-6} M to 6.1 x 10^{-4} M of L-Met and a linear regression values and correlation coefficient as *I*pa (V) = 0.4352x + 0.0267 and R^2 = 0.9983 respectively. The comparison of analytical parameters such as concentration range, and limit of detection of L-Met with other modified electrodes compared to previous reports (Table 1).

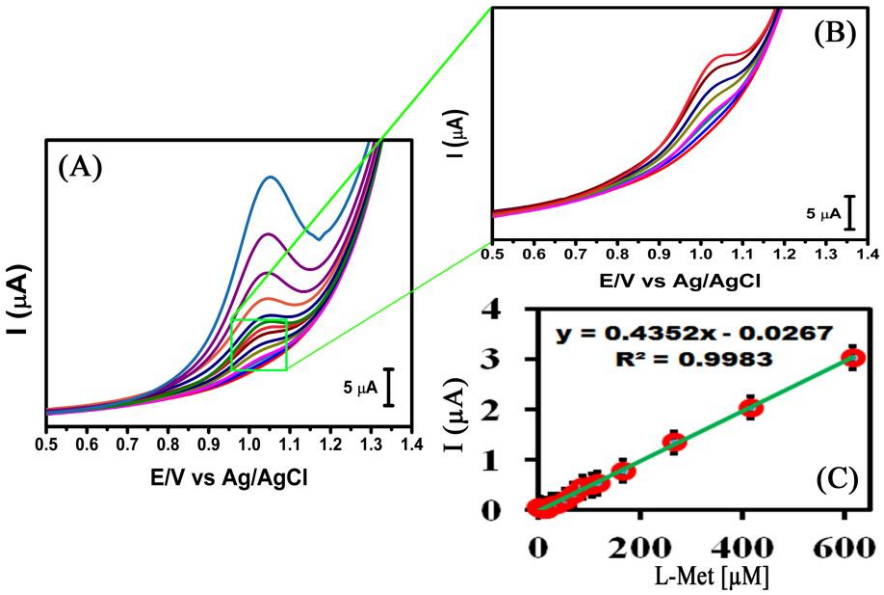

Figure 7. DPVs obtained of (A) Mn_2O_3/SPCE different concentrations from 1.0 x 10^{-6} M to 6.1 x 10^{-4} M (B) lower concentrations, and (C) calibration curve of peak current versus the concentrations of L-Met in N_2 saturated PBS at the scanning rate of 50 mV s^{-1}.

Table 1. Similarity parameters for detection of L-Met at a various modified electrode.

Electrode Substrate	Linear range (M)	Detection limit (M)	Ref
ETAP-Cu(II)/GCE	5.0 x 10^{-5} – 5.0 x 10^{-4}	2.7 x 10^{-8}	34
PAMT/GCE	1.0 x 10^{-7} – 1.0 x 10^{-4}	4.1 x 10^{-10}	35
Au-Cys/GCE	1.0 x 10^{-6} – 1.0 x 10^{-4}	5.9 x 10^{-7}	36
Bi (V) -PbO_2/Au	–	1.0 x 10^{-3}	41
SWCNT-NiCNT/GCE	1.0 x 10^{-5} – 1.0 x 10^{-4}	4.5 x 10^{-6}	42
Ni/CCE	2.0 x 10^{-6} – 9.0 x 10^{-5}	2.0 x 10^{-6}	43
Rh_2POM/CE	–	7.3 x 10^{-4}	44
GO/SPCE	2.0 x 10^{-6} – 9.6 x 10^{-5}	1.8 x 10^{-7}	45
$Co(OH)_2$/GCE	2.5 x 10^{-1} – 1.2 x 10^{0}	1.6 x 10^{-4}	46
F-C60/GCE	1.0 x 10^{-5} – 1.0 x 10^{-3}	8.2 x 10^{-6}	47
Mn_2O_3/SPCE	**1.0 x 10^{-6} – 6.1 x 10^{-4}**	**1.0 x 10^{-9}**	**This work**

ETAP-Cu(II) = Electropolymerized film 1,8,15,22-tetraaminophthalocyanato-Cu(II), PAMT = Poly (3-amino-5-mercapto-1,2,4-triazole), Au-Cys = Colloidal-gold cysteamine, PMV = Poly (methyl violet), Pt = Platinum, CPE = Carbon paste electrode, Ru^{II} Den = Ruthinium(II) dendrimer, CE = Carbon-composite electrode, Bi(V)-PbO_2 = Bi(V) doped PbO_2 film, CCE = Carbon ceramic electrode, SWCNT-NiCNT = Single-wall carbon nanotube and nickel-carbon nanotube, $Co(OH)_2$ = Cobalt hydroxide, Full-C60 = Fullerene-C60, GO = Graphene Oxide, SPCE = Screen printed carbon electrode.

3.6. Accumulation time, reproducibility, and operational stability

To study the impacts of an accumulation time for the electro-catalytic oxidation of L-Met, the CV curve were reported for Mn_2O_3/SPCE in the presence of 200 μM L-Met in 0.05 M PBS (pH 7) with a scanning rate of 50 mV s^{-1} as shown in Fig. 8A. Additionally, the oxidation peak currents for L-Met were recorded for the different accumulation time started from 0 to 210 s, where the higher electro-catalytic oxidation peak current was detected for 90 s. Therefore, the modified electrode was optimized with suitable accumulation time was considered to be 90 s for a proficient electro-catalytic oxidation of L-Met molecule. Reproducibility of the sensor, was determined by using five different Mn_2O_3/SPCE were modified and verified towards 200 μM L-Met. The attained reproducibility results are displayed in Fig. 8B which reveals that the Mn_2O_3/SPCE have an excellent reproducible ability, and the electrode can be used for exact detection of L-Met. The CV response of 100 nonstop cycles of the Mn_2O_3/SPCE in the absence and presence of L-Met is shown in Fig. 8C, D. The results indicated Mn_2O_3/SPCE has long-term stability [48].

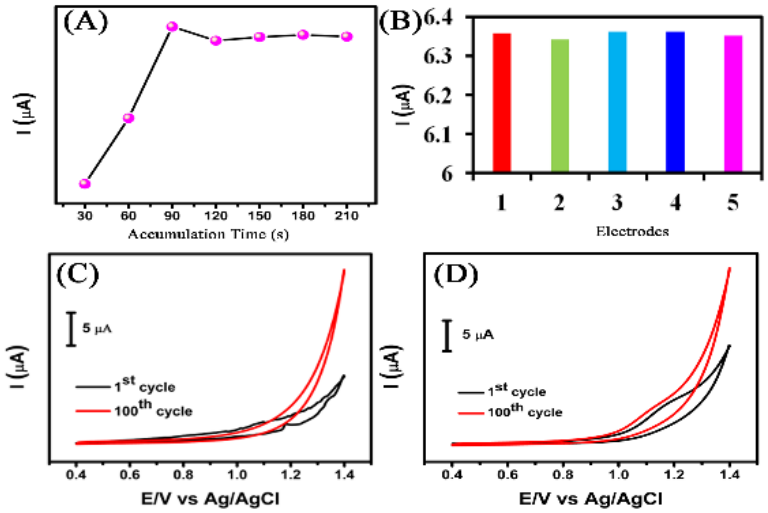

Figure 8. CV response of (A) accumulation time (B) reproducibility (C) operational stability of 100 nonstop cycles without, and (D) with L-Met of Mn_2O_3/SPCE N_2 saturated PBS at the scanning rate of 50 mV s^{-1}.

3.7. Real sample analysis

The suggested L-Met sensor was additional confirmed using real sample analysis, such as a Wild Salman, and Shrimp were found from a local market in Taipei, Taiwan. The biological samples were crushed with a little amount of water, and the extracted was ultra-centrifuged aforementioned to the real sample studies. The sample extracts were spiked by L-Met in PBS solution (10 mL), as shown in Fig. 9A, C. Plot between the concentration of biological samples, and current are shown in Fig. 9B, D. Obviously, the Mn_2O_3/SPCE is entirely appropriate for real sample analysis, the equivalent DPV results are shown in Table 2.

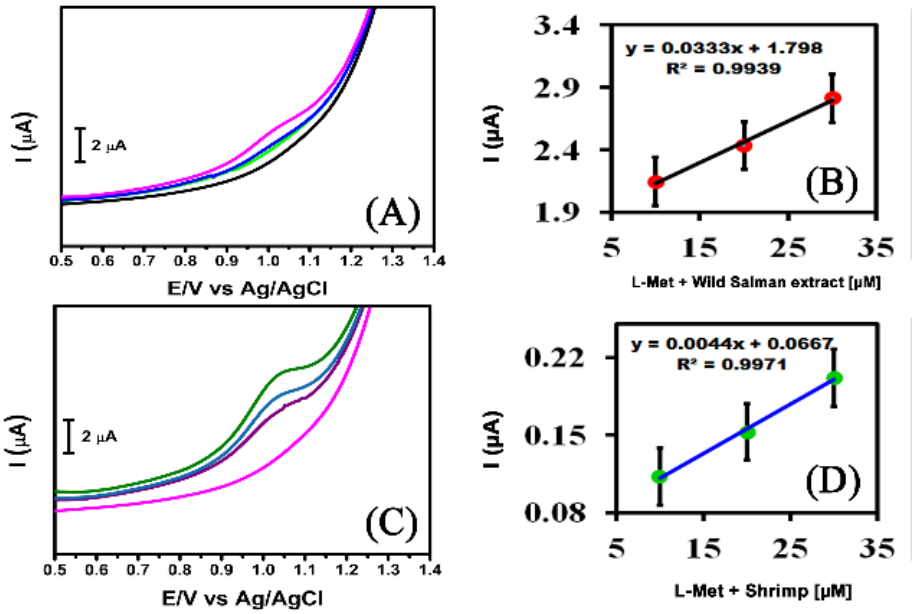

Figure 9. DPV curves of the Mn_2O_3/SPCE in (A) Wild Salman (C) Shrimp samples containing L-Met with PBS (pH 7), and (B) plots of oxidation current versus L-Met + Wild salman extract and (D) plots of oxidation current versus L-Met + Shrimp extract were obtained at a scanning rate of 50 mV s^{-1}.

Table 2. Real sample analysis of L-Met using spiked method Mn_2O_3/SPCE. (n = 3)

S.No	Samples	Added (µM)	Found (µM)	Recovery (%)	RSD (%)
1	Wild Salman	10	9.59	95.9	2.25
		20	21.45	107.25	3.61
		30	30.26	100.86	3.58
2	Shrimp	10	9.23	92.3	2.15
		20	20.95	104.75	2.95
		30	25.32	84.4	4.12

RSD = Relative standard deviation

3.8. Catalytic reduction of p-NP

To evaluate the catalytic activity of Mn_2O_3 during reduction of p-NP, test reactions were carried out by mixing aqueous solution of p-NP (1 x 10^{-4} M) with a reducing agent ($NaBH_4$) (1 M). When addition of appropriate amount of Mn_2O_3, into the reaction, and it was observed by UV-Vis spectroscopy. In brief, while addition of $NaBH_4$ into the aqueous p-NP (light yellow color), the reaction solution suddenly undertook from 317 to 400 nm, signifying the formation of p-Nitrophenolate ion, as shown in Fig. 10A. Without Mn_2O_3 the reduction efficiency was very low (Fig. 10B), while adding ca. 1 mg of Mn_2O_3 into the above reaction mixture, a reliable decrease happened in the intensity of the absorption peak at 400 nm with time, representing a consecutive reduction of p-Nip (Fig. 10C). This is accompanied by the presence of a new absorption peak at 300 nm, whose intensity

gradually improved with time, showing the expected formation of p-Aminophenol (p-AP). Moreover, even in the existence of strong reducing agent $NaBH_4$, the wavelength, and intensity of the peak responsible for p-Nip (at 400 nm) stayed closely unmoved in the absence of a Mn_2O_3.

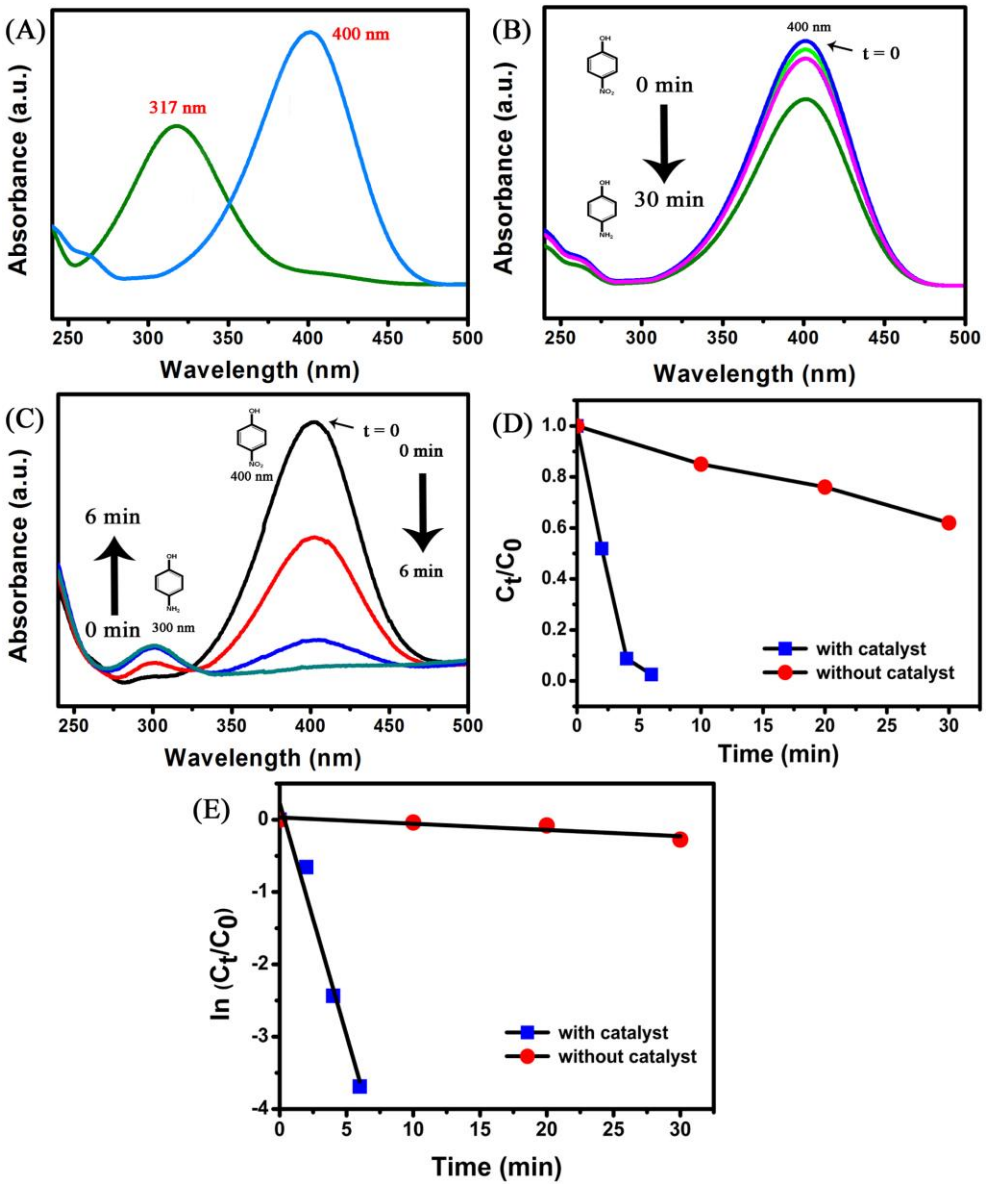

Figure 10. (A) UV-Vis spectra obtained from aqueous p-NP before (green curve) and after (blue curve) the addition of $NaBH_4$ solution, (B) Absorption spectra of aqueous solution containing p-NP (1×10^{-4} M) and $NaBH_4$ (1 M) without Mn_2O_3, (C) with Mn_2O_3 (D) Plots of C_t/C_0 versus reaction time (min), and (F) Plots of ln (C_t/C_0) versus reaction time (s) for the reduction of p-NP with Mn_2O_3.

Based on a before reported scheme [27], the mechanism for the reduction of p-NP in the occurrence of $NaBH_4$ over the Mn_2O_3 is demonstrated in Scheme 3. Consequently, the catalytic reduction of p-NP over Mn_2O_3 is motivated by the electron transfer from BH_4^- to p-NP through adsorption of the reactant molecules onto the surfaces of the Mn_2O_3 (Step I). The catalytic reduction

activity is known to depend on the surface area of the Mn_2O_3 as well as the mass transfer resistant to the reactant. The final clearly assistances from the mesoscopic properties such as surface area, pore volume, and porous size of the Mn_2O_3. The catalytic reduction of p-NP, which is the rate-determining step is activated by the relations of the adsorbed p-NP with hydrogen atoms bound on the active surfaces of Mn_2O_3 (Steps II and III). As a result of reduction reaction, p-AP is formed, followed by the desorption of product from the Mn_2O_3 (Step IV) and reactivation of the Mn_2O_3 system [27].

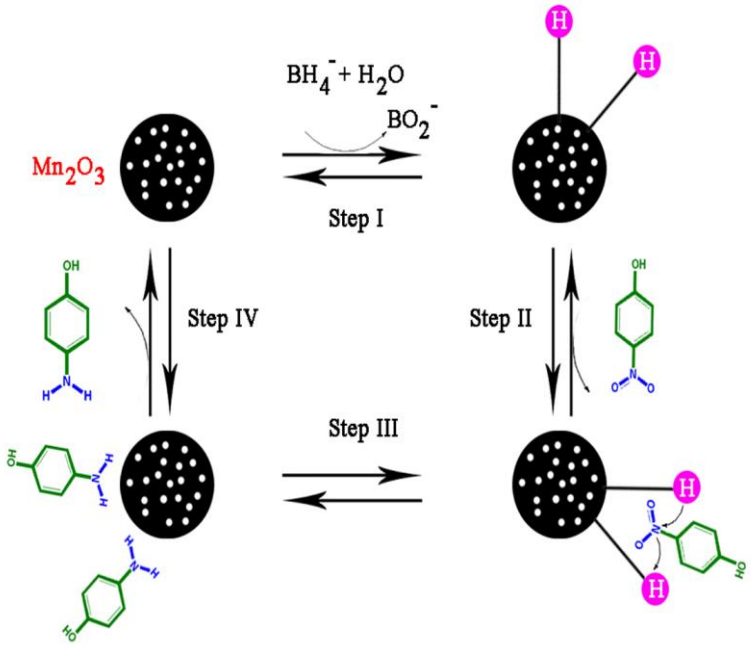

Scheme 3. The suggested mechanism of the catalytic reduction of the 4-NP by $NaBH_4$ using Mn_2O_3.

4. CONCLUSIONS

In conclusion, we have reported electrochemical determination of L-Met and catalytic reduction of p-Nitrophenol. From the electrochemical study, the results revealed the bare SPCE showed a little bit oxidation peak for L-Met whereas, the modified working electrode displayed a well-defined oxidation peak, and improved its oxidation current. Using the DPV method, a detection limit is about 1.0×10^{-9} M (S/N=3) was attained. The modified working electrode indicated a good recovery for L-Met in Wild Salman, and Shrimp, representing that the current technique may be used for practical applications. In particular, Mn_2O_3 catalyst were found capable of reducing p-Nitrophenol to p-Aminophenol with extraordinary reactivity in the presence of $NaBH_4$ as the reducing agent. From UV-Vis spectroscopy results the complete reduction of p-NP to p-AP can be reached within 5-6 min even with a catalyst loading of only 1 mg. The benefits of the current modified working electrode are ease in alteration, no need to preserve the electrode in the refrigerator or buffer solution, and highly stable, and catalyst has excellent property of reduction of p-NP.

ACKNOWLEDGEMENTS
The authors gratefully acknowledge the financial support of the National Taipei University of Technology, and Chang Gung Memorial Hospital Joint Research Program(NTUT-CGMH-107-No.04), (CORPG1H0011). The National Science Council, and The Ministry of Education, Taiwan supported this work. We would also like to acknowledge The Ministry of Science and Technology, Taiwan (MOST 106-2113-M-027-003) for its financial support.

References

1. S. Ching, D. A. Kriz, K. M. Luthy, E. C. Njagi and S. L. Suib, *Chem. Commun*., 47 (2011) 8286.
2. C. Yuan, L. Hou, L. Yang, D. Li, L. Shen, F. Zhang and X. Zhang, *J. Mater. Chem.*, 21 (2011) 16035.
3. L. Espinal, W. Wong-Ng, J. A. Kaduk, A. J. Allen, C. R. Snyder, C. Chiu, D. W. Siderius, L. Li, E. Cockayne, A. E. Espinal and S. L. Suib, *J. Am. Chem. Soc*., 134 (2012) 7944.
4. A. K. Sinha, M. Basu, M. Pradhan, S. Sarkar, Y. Negishi, T. Pal, *J. Phys. Chem. C* 114 (2010) 21173.
5. J. Cao, Q. Mao and Y. Qian, *J. Solid State Chem*., 191 (2012) 10.
6. Y. Ren, Z. Ma, L. Qian, S. Dai, H. He and P. G. Bruce, *Catal. Lett*., 131 (2009) 146.
7. Y. Wang, Y. Wang, D. Jia, Z. Peng, Y. Xia and Zheng, *Nano Lett*., 14 (2014) 1080.
8. Y. Zhang, Y. Yan, X. Wang, G. Li, D. Deng, L. Jiang, C. Shu and C. Wang, *Chem. – Eur. J*., 20 (2014) 1.
9. Y. Qiao, Y. Yu, Y. Jin, Y. –B. Guan and C. –H. Chen, *Electrochim. Acta* 132 (2014) 323.
10. Y. Dai, H. Jiang, Y. Hu and C. Li, *RSC Adv*., 3 (2013) 19778.
11. Y. Cai, S. Liu, X. Yin, Q. Hao, M. Zhang, T. Wang, *Phys. E* 43 (2010) 70.
12. M. –W. Xu, Y. –B. Niu, S. Bao and C. M. Li, *J. Mater. Chem. A* 2 (2014) 3749.
13. (a) J. J. Cao, Y. Zhu, K. Bao, L. Shi, S. Liu and Y. Qian, *J. Phys. Chem. C* 113 (2009) 17755; (b) L. Chang, L. Mai, X. Xu, Q. An, Y. Zhao, D. Wang and X. Feng, *RSC Adv*. 3 (2013) 1947.
14. Y. Deng, Z. Li, Z. Shi, H. Xu, F. Peng and G. Chen, *RSC Adv*. 2 (2012) 4645.
15. X. Zhang, Y. Qian, Y. Zhu and K. Tang, *Nanoscale* 6 (2014) 1725.
16. P. Pal, A. K. Giri, S. Mahanty, A. B. Panda, *CrystEngComm*., 16 (2014) 10560.
17. H. Y. Lee and J. B. Goodenough, *J. Solid State Chem*., 144 (1999) 220.
18. S. –C. Pang, M. A. Anderson and T. W. Chapman, *J. Electrochem. Soc*., 147 (2000) 444.
19. Y. U. Jeong and A. Manthiram, *J. Electrochem. Soc*., 149 (2002) A1419.
20. J. –K. Chang and W. –T. Tsai, *J. Electrochem. Soc*., 150 (2003) A1333.
21. C. –C. Hu and C. –C. Wang, *J. Electrochem. Soc*., 150 (2003) A1079.
22. H. Y. Lee, S. W. Kim and H. Y. Lee, *Electrochem. Solid State Lett*., 4 (2001) A19.
23. M. Toupin, T. Brousse and D. Belanger, *Chem. Mater*., 16 (2004) 3184.
24. T. E. Moore, M. Ellis and P. W. Selwood, *J. Am. Chem. Soc*., 72 (1950) 856.
25. J. W. Long, A. L. Young and D. R. Rolison, *J. Electrochem. Soc*., 150 (2003) A1161.
26. R. N. Reddy and R. G. Reddy, *J. Power Sources* 124 (2003) 330.
27. S. –J. Bao, B. –L. He, Y. –Y. Liang, W. –J. Zhou and H. –L. Li, *Mater Sci Eng A* 397 (2005) 305.
28. J. Liu, Q. Sheng, F. Nie and J. Zheng, *J. Electrochem. Soc*., 161 (2014) B225.
29. A. Puangjan, S. Chaiyasith, S. Wichitpanya, S. Daengduang and S. Puttota, *J. Electrochem. Soc*., 782 (2016) 192.
30. J. Chen, W. –D. Zhang and J. –S. Ye, *Electrochem Commun*., 10 (2008) 1268.
31. D. Voet and J. G. Voet, *Biochemistry*, II edn, Wiley, New York (1995).
32. M. Salimi and Roushani, *Electroanal*., 18 (2006) 2129.
33. T. Hoshi and S. H. Heinemann, *J. Physiol*., 531 (2001) 1.
34. M. E. Tess and J. A. Cox, *Electroanal*., 10 (1998) 1237.
35. L. Ozcan and Y. Sahin, *Sens. Actuators B* 127 (2007) 362.

36. N. D. Popovic and D. C. Johnson, *Electroanal*., 11 (1999) 934.
37. K. S. Pugazhvadivu, K. Ramachandran, and Tamilarasan, *Physics Procedia* 49 (2013) 205.
38. Q. Javed, F. P. Wang, M. Y. Rafique, A. M. Toufiq, Q. S. Li, H. Mahmood and W. Khan, *Nanotechnology* 23 (2012) 1.
39. S. Zhan, D. Zhu, M. Qiu, H. Yu and Y. Li, *RSC Adv*., 5 (2015) 29353.
40. F. Jiao, A. Harrison, A. H. Hill and P. G. Bruce, *Adv. Mater*., 19 (2007) 4063.
41. H. Xu, W. Zhang, W. Zhu, D. Wang, J. Ye, K. Yamamoto and L. Jin, *Anal. Chim. Acta* 545 (2005) 182.
42. O. Daniel, *BJU Int*., 26 (1954) 153.
43. P. Kalimuthu and S. A. John, *Electrochem. Commun*., 11 (2009) 367.
44. S. B. Revin and S. A. John, *Electrochim. Acta* 56 (2001) 8934.
45. R. Sasikumar, P. Ranganathan, S. –M. Chen, T. Kavitha, S. –Y. Lee, T. –W. Chen and W. –H. Chang, *Int. J. Electrochem. Sci*. 12 (2017) 4077.
46. P. Kalimuthu and S. A. John, *Electrochim. Acta* 55 (2009) 183.
47. J. G. Velasco, *Electroanal*., 9 (1997) 880.
48. R. Sasikumar, M. Govindasamy, S. –M. Chen, Y. –C. Liu, P. Ranganathan and S. –P. Rwei, *J. Colloid Interface Sci*., 504 (2017) 626.